




Multifunctional Involvement of a C₂H₂ Zinc Finger Protein (PbZfp) in Malaria Transmission, Histone Modification, and Susceptibility to DNA Damage Response

Anusha M. Gopalakrishnan,^{a*} Ahmed S. I. Aly,^a L. Aravind,^b  Nirbhay Kumar^a

Department of Tropical Medicine, School of Public Health and Tropical Medicine, Vector-Borne Infectious Diseases Research Center, Tulane University, New Orleans, Louisiana, USA^a; National Center for Biotechnology Information, NIH, Bethesda, Maryland, USA^b

ABSTRACT In sexually reproducing organisms, meiosis is an essential step responsible for generation of haploid gametes from diploid somatic cells. The quest for understanding regulatory mechanisms of meiotic recombination in *Plasmodium* led to identification of a gene encoding a protein that contains 11 copies of C₂H₂ zinc fingers (ZnF). Reverse genetic approaches were used to create *Plasmodium berghei* parasites either lacking expression of full-length *Plasmodium berghei* zinc finger protein (PbZfp) (knockout [KO]) or expressing PbZfp lacking C-terminal zinc finger region (truncated [Trunc]). Mice infected with KO parasites survived two times longer ($P < 0.0001$) than mice infected with wild-type (WT) parasites. In mosquito transmission experiments, the infectivity of KO and Trunc parasites was severely compromised (>95% oocyst reduction). KO parasites revealed a total lack of trimethylation of histone 3 at several lysine residues (K4, K27, and K36) without any effect on acetylation patterns (H3K9, H3K14, and H4K16). Reduced DNA damage and reduced expression of topoisomerase-like Spo11 in the KO parasites with normal Rad51 expression further suggest a functional role for PbZfp during genetic recombination that involves DNA double-strand break (DSB) formation followed by DNA repair. These findings raise the possibility of some convergent similarities of PbZfp functions to functions of mammalian PRDM9, also a C₂H₂ ZnF protein with histone 3 lysine 4 (H3K4) methyltransferase activity. These functions include the major role played by the latter in binding recombination hotspots in the genome during meiosis and trimethylation of the associated histones and subsequent chromatin recruitment of topoisomerase-like Spo11 to catalyze DNA DSB formation and DMC1/Rad51-mediated DNA repair and homologous recombination.

IMPORTANCE Malaria parasites are haploid throughout their life cycle except for a brief time period when zygotes are produced as a result of fertilization between male and female gametes during transmission through the mosquito vector. The reciprocal recombination events that follow zygote formation ensure orderly segregation of homologous chromosomes during meiosis, creating genetic diversity among offspring. Studies presented in the current manuscript identify a novel C₂H₂ ZnF-containing protein exhibiting multifunctional roles in parasite virulence, mosquito transmission, and homologous recombination during meiosis. Understanding the transmission biology of malaria will result in the identification of novel targets for transmission-blocking intervention approaches.

KEYWORDS DNA damage, epigenetic modification, malaria transmission, zinc finger proteins

Received 25 July 2017 Accepted 27 July 2017 Published 29 August 2017

Citation Gopalakrishnan AM, Aly ASI, Aravind L, Kumar N. 2017. Multifunctional involvement of a C₂H₂ zinc finger protein (PbZfp) in malaria transmission, histone modification, and susceptibility to DNA damage response. *mBio* 8:e01298-17. <https://doi.org/10.1128/mBio.01298-17>.

Editor Diane E. Griffin, Johns Hopkins Bloomberg School of Public Health

This is a work of the U.S. Government and is not subject to copyright protection in the United States. Foreign copyrights may apply.

Address correspondence to Nirbhay Kumar, nkumar@tulane.edu.

* Present address: Anusha M. Gopalakrishnan, Molecular Genetics and Microbiology, Duke Medical School, Durham, North Carolina, USA.

This article is a direct contribution from a Fellow of the American Academy of Microbiology. Solicited external reviewers: Richard Carter, University of Edinburgh; Debopam Chakrabarty, Burnett School of Biomedical Sciences.

Malaria, a disease caused by blood infection with protozoan parasites of the genus *Plasmodium*, remains a major public health challenge, with an estimated 214 million cases and ~438,000 deaths recorded worldwide in 2015 (1). An effective vaccine to control malaria has not been developed; antigenic variation, genetic diversity, and antimalarial drug resistance continue to impede control efforts. The lifecycle of the parasite alternates between a vertebrate host and an invertebrate mosquito vector. For continuation of the life cycle from one host to another, it is essential for the parasites to differentiate and develop into sexual stages. *Plasmodium* organisms are haploid throughout their life cycle except for the brief stage postfertilization within the mosquito midgut when haploid gametes fuse to form diploid zygotes. Within hours, these undergo meiosis and develop into ookinetes.

Studies in the malaria parasite *Plasmodium falciparum* have provided evidence of a process that begins with frequent random mating involving haploid gametes of genetically distinct parasite clones. The diploid zygote then undergoes meiotic division, and genetic recombination during meiosis contributes to the genetic diversity of the parasite, as with other sexually reproducing eukaryotes (2–6). Homologous recombination (HR) is central to meiosis in almost all organisms, and reciprocal recombination events, also known as crossing-over events, lead to the orderly segregation of homologous chromosomes. Recombination during meiosis is also responsible for the creation of genetic diversity among offspring of diverse parental backgrounds (7). In mammalian cells, crossing-over events during meiotic recombination are not distributed randomly but are clustered in short-interval regions along chromosomes called “hotspot” (8).

Studies on identification and genome-wide mapping of recombination (9–11) have revealed a correlation between hotspot activity and enrichment of trimethylated histone 3 at lysine 4 (H3K4me3) (12, 13). Further studies in mammals have identified PRDM9, a meiosis-specific chromatin-modifying protein, as the key determinant of recombination hotspots and a master transcription regulator of entry into meiosis (14–17). The PRDM9 protein contains a C-terminal module comprised of multiple C₂H₂-type zinc fingers (ZnF) which binds the degenerate 13-bp motif that was previously found to be associated with ~40% of human hotspots, formation of double-strand breaks (DSB), and recruitment of the recombination machinery leading to exchange of chromosomal material and DNA repair. Additionally, the ZnF domain (Zfd) in PRDM9 is fused to a SET domain which catalyzes the trimethylation of histone 3 lysine 4 (H3K4) and histone 3 lysine 36 (H3K36) associated with the hotspots (18, 19). The SET domain initially characterized in *Drosophila* is an evolutionarily well-conserved domain associated with many chromosomal proteins and with proteins necessary for histone lysine trimethylation in mammalian cells (20).

The C₂H₂-type Zfd, represented by two cysteine and two histidine residues separated by ~12 amino acids acting as ligands to a zinc atom, are widespread in most DNA-binding proteins (21, 22). In animals, proteins with multiple C₂H₂ ZnFs are transcription factors regulating gene expression and acting during cell differentiation and development. Binding of C₂H₂ ZnF proteins to DNA often helps recruit other proteins which mediate epigenetic changes, including posttranslational modifications of histones. These include histone methylases as well as enzymes catalyzing demethylation of H3K4me3 and other histone methyl transferases transferring methyl groups to H3K9 and H3K27. Depending upon the sites methylated, histone methylation is involved in both repression and activation of transcription (23–25). For example, trimethylation of K4 in H3 (HeK4me3) is associated with activation, whereas trimethylation of K9 (H3K9me3) and trimethylation of K27 (H3K27me3) are generally associated with transcription repression (20, 26). In contrast, acetylation of histone lysine residues relaxes chromatin structures, leading to increased transcriptional and gene expression activities in the cell.

Meiotic recombination involves a series of orchestrated and programmed biochemical events beginning with DNA DSB and DNA repair (27–29). Genetic mapping and hotspot identification have also been performed in *Plasmodium* spp. (30–33). Previously, our laboratory identified and investigated the role of molecules involved in HR. These

include *P. falciparum* Rad51 (PfRad51), *P. falciparum* Rad54 (PfRad54), and two types of *P. falciparum* replication protein A1 (PfRPA1L and PfRPA1S) involved in DNA strand exchange and DNA-DSB repair processes in erythrocytic stages of *P. falciparum* (34–36) and Dmc1 (disrupted meiotic cDNA homolog, a meiotic recombinase) involved in the sporogonic life cycle of *P. berghei* (a murine malaria parasite) ensuing after meiotic nuclear division in developing zygotes in the mosquito midgut (37). However, it is not known how recombination machinery is recruited to the site of DNA damage and whether *Plasmodium* employs molecular mechanisms similar to those deployed in mammals for recognition of putative recombination hotspots. In this study, we investigated if *Plasmodium* utilizes a molecule analogous to mammalian PRDM9, particularly with respect to hotspot choice, hotspot-associated H3K4 trimethylation, and DNA-DSB repair mechanisms.

RESULTS

Characteristic features of PbZfp. While proteins with runs of multiple (>3) instances of C₂H₂ ZnF are common in animals, the *P. berghei* Zfp (PbZfp) protein is the only such example conserved across *Plasmodium* species: PbANKA_06077 in *P. berghei*, PF3D7_1209300 in *P. falciparum*, PKH_13092 in *P. knowlesi*, Py17X_0610200 in *P. yoelii*, and PVX_084495 in *P. vivax*. The protein is comprised of a poorly conserved N-terminal low-complexity region and a C-terminal region with 11 C₂H₂ ZnFs, which is where the sequence similarity is most pronounced. The C₂H₂ ZnFs are arranged in an initial run of 3 ZnFs followed by a disordered poorly conserved linker connecting them to the remaining 8 ZnFs. Unlike the animal PRDM9 protein, PbZfp lacks the methyltransferase SET domain and does not have KRI domains typical of the members of the KRAB family of animal C₂H₂ ZnF proteins. Thus, while not directly related to these animal proteins, PbZfp shows an unusual resemblance to animal C₂H₂ ZnF proteins in having a multiplicity of C₂H₂ Zfd (22). Notably, orthologs of PbZfp exhibiting greater sequence divergence are also seen in other *Apicomplexa* species, such as piroplasms (e.g., *Theileria* spp.), coccidians (e.g., *Toxoplasma* spp.), and *Cryptosporidium* spp. Additionally, bioinformatics analysis predicted three potential phosphorylation sites in the *P. falciparum* homolog of PbZfp, a result which was experimentally validated by phosphoproteome analysis of erythrocytic asexual life cycle stages, demonstrating phosphorylation at serine residues 512, 596, and 1230 (38). PbZfp conservation in a single copy across *Apicomplexa* is unlike the more lineage-specific conservation patterns of transcription factors (39). Further, the presence of a run of multiple C₂H₂ ZnFs indicates that the protein might contact an extended binding site as is typical of recombination hotspots. These observations pointed to potential roles in addition to or beyond that of a conventional transcription factor and prompted us to investigate if it might play a role in recombination.

Targeted disruption of the *PbZfp* gene. To study the biological role of PbZfp, we employed two *PbZfp* gene disruption strategies. In the first, we generated loss-of-function parasite clones by targeting the full-length endogenous gene (Fig. 1B, panel III) using an insertion plasmid (Fig. 1B, panel I). As shown in panel IV of Fig. 1B, HR within the 5' *utr* and 3' *utr* regions of the genomic locus (Fig. 1B, panel III) and the targeting plasmid was expected to result in the disruption of genomic *PbZfp*. We also sought to generate parasites expressing truncated (Trunc) PbZfp, lacking the C-terminal C₂H₂ ZnFs (Fig. 1A, panel II). A truncation plasmid (Fig. 1B, panel II) was designed to introduce a stop codon within the coding sequence at the start of the Zfd. Panel V of Fig. 1B shows the expected locus in the truncated parasites after HR within the coding sequence and the 3' *utr* regions of the genomic locus and the targeting plasmid. Parasites obtained from successful transfection were used for further cloning, and two independent clones of each type (knockout [KO] and Trunc) were employed in various studies. Insertion-specific diagnostic PCRs were done using different primer combinations (see Fig. S1 in the supplemental material; locations of primers are indicated in Fig. 1, and sequences are listed in Table S1 in the supplemental material). Integration at the 5' end was confirmed using primer pair 815/921 (panel A of Fig. S1 shows an

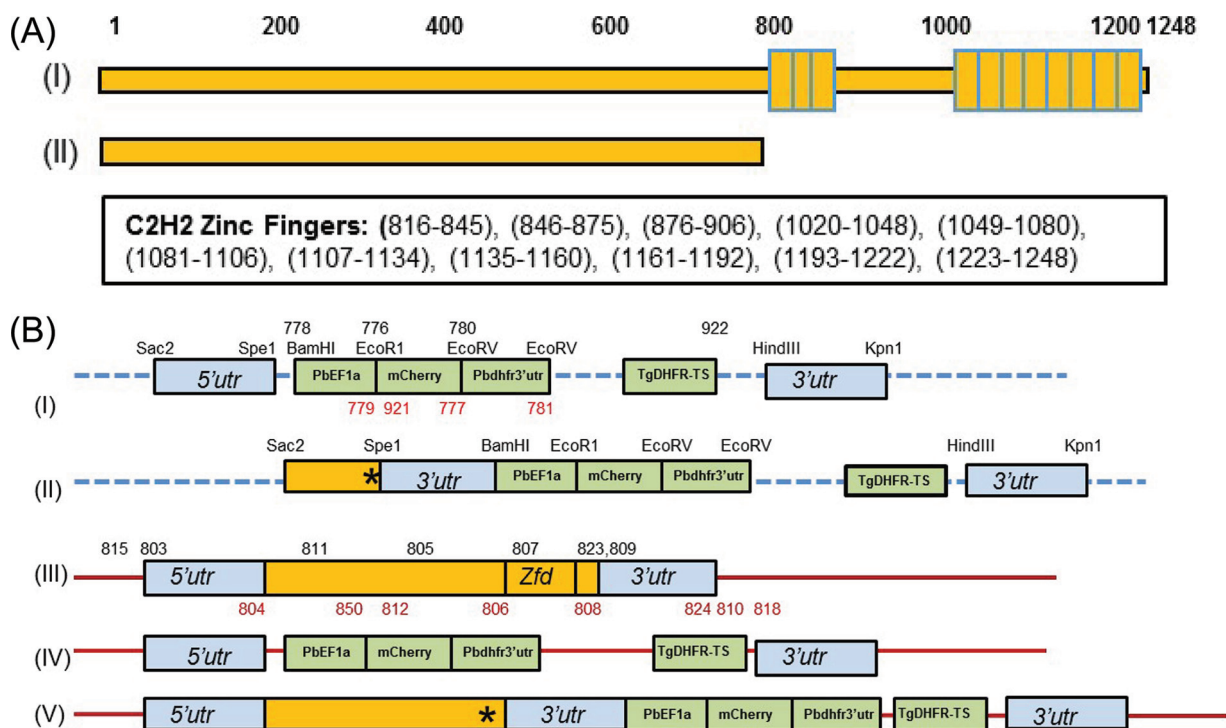


FIG 1 Schematic of PbZfp and gene-targeting plasmids. PbZfp was identified by PSI-BLAST sequence profiling for C2H2 ZnF and BLAST analysis of PlasmoDB database entries using the protein sequence of mouse PRDM9 as a query. (A) Schematic of PbZfp protein (1,248 amino acids) and relative positions of 11 zinc fingers (boundaries are indicated in the text box), identified by PSI-BLAST analysis (panel I). A schematic of truncated PbZfp protein lacking Zfd expression is shown in panel II. (B) Schematic of targeting plasmids and parasite genomic locus, before and after transfection. Details of sequential steps used to construct plasmids are given in Materials and Methods. Key features of the plasmids used to generate PbZfp knockout and truncated parasites are shown in panels I and II, respectively. In the truncation plasmid shown in panel II, a stop codon (*) was inserted near the 5' end of the sequence coding for the Zfd. Various restriction sites are also identified. The wild-type *PbZfp* genomic locus is represented in panel III. Panel IV shows the genomic locus in *PbZfp* knockout (KO) parasites after homologous recombination events at the 5'utr and 3'utr sequences present in the targeting plasmid (panel I) and the wild-type genomic locus (panel III). Panel V shows the expected genomic locus after homologous recombination events at the PbZfp coding sequence and 3'utr sequences present in the plasmid (panel II) and wild-type genomic locus (panel III). Various oligonucleotide primers used for PCR amplification and characterization are shown by numbers (panels I and III). Forward primers are indicated in black numbers and reverse primers in red.

expected size of ~1.7 kb for KO parasites and panel D an expected size of ~3.9 kb for Trunc parasites). Integration at the 3' end was confirmed using primer pair 922/818 (see panel B of Fig. S1 for KO and panel E for Trunc parasites, showing an expected size of ~1.0 kb). Panel C of Fig. S1 also shows PCR results for genomic loci in wild-type (WT) parasites (5,398 bp) and in KO parasites (8,069 bp).

Loss of expression of *PbZfp* in disrupted parasites revealed by RT-PCR. Next, we demonstrated the absence of expression of full-length *PbZfp* in the KO parasites. Reverse transcriptase PCR (RT-PCR) performed using primers 811/812 revealed an 850-bp transcript band in WT parasites, whereas no band was seen in the KO parasites (Fig. 2A). In parallel, we tested RNA from WT and *PfZfp* KO parasites for expression of Rad51 and detected the presence of an ~500-bp transcript in both, ruling out any nonspecific gene-targeting event. Results of reactions performed in the absence of a reverse transcriptase step were negative. We also tested gene expression in the Trunc parasites. Similarly to KO parasites, the results obtained using primers 807/808 with Trunc parasites were negative, whereas WT parasites showed an expected 650-bp fragment (Fig. 2B). Interestingly, when primers 807/810 were employed, the Trunc and WT parasites revealed ~500-bp and ~1,000-bp fragments, respectively (Fig. 2C), establishing the expression pattern for *PbZfp* truncated by removing the Zfd coding region. Expression of truncated PbZfp (upstream sequence encoding the N-terminal region) was further confirmed by positive RT-PCR results obtained using primer pair 811/812 and a smaller RT-PCR band in Trunc parasites obtained using primers 811/810 (data not shown).

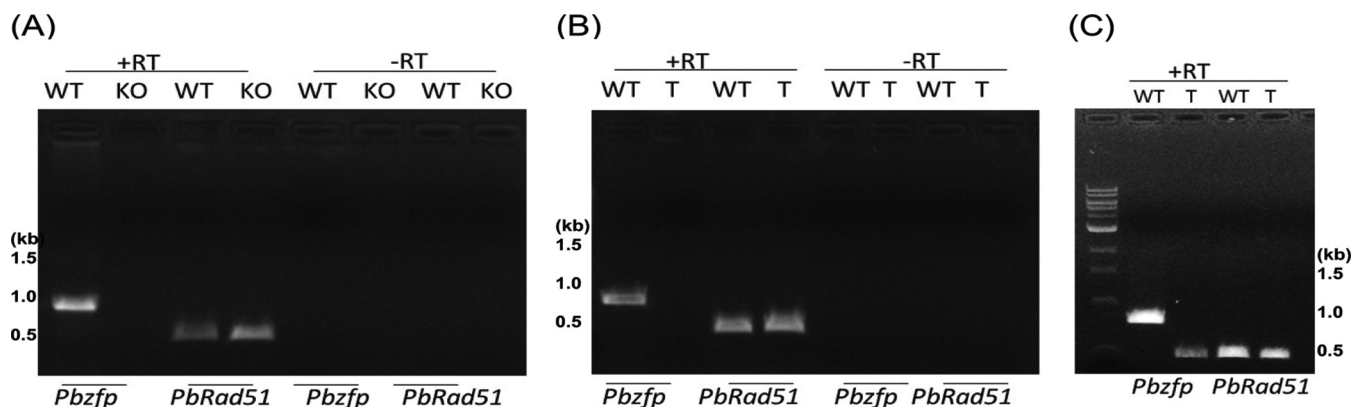


FIG 2 RT-PCR demonstration of *pbzfp* expression. Total RNA from WT, KO (A), and truncated (B and C) parasites was reverse transcribed (+RT lanes), and cDNAs were used as the templates for PCR amplification. RNAs without reverse transcription (–RT lanes) were used as negative controls. Primer pairs used to confirm *PbZfp* expression by RT-PCR were 811/812 (A), 807/808 (B), and 807/810 (C). Primers 610/857 were used for *PbRad51* expression in the WT, KO, and Trunc parasites (panels A, B, and C). Sequences of various primers used are described in Table S1. All the samples were also tested using primers for an unrelated gene (*PbRad51*) to establish the specificity and quality of RNA samples.

Asexual- and sexual-stage growth and transmission competence of *PbZfp* KO and Trunc parasites.

To evaluate whether genetic disruption or truncation of *PbZfp* would affect various life cycle parameters, we followed the asexual growth kinetics of the WT, KO, and Trunc parasites. Swiss Webster mice ($n = 3$ per group) were infected intravenously (i.v.) with 10^5 parasites in four independent experiments, and parasitemia was monitored daily in the infected mice. The asexual growth kinetics of the WT, KO, and Trunc parasites were comparable, with the exception that mice infected with KO parasites survived significantly longer (Fig. 3A). Figure 3B shows Kaplan-Meier survival plots for mice infected with WT, KO, and Trunc parasites. Mice infected with KO parasites lived nearly twice as long as those infected with WT parasites. Even mice infected with Trunc parasites showed a survival advantage over WT-infected mice. These data implicate *PbZfp* as a potential determinant of parasite virulence.

Next, to examine the transmission competence of WT, KO, and Trunc parasites, Swiss-Webster mice (3 mice/group) were infected (i.v.) with 10^5 WT, KO, or Trunc parasites. A drop of blood from infected mice was used to examine exflagellation of male gametocytes, and mice were used to infect *Anopheles stephensi* mosquitoes on day 4 postinfection. At 9 to 11 days postfeeding, mosquitoes were dissected, individual midguts were stained with 0.1% mercurochrome, and oocysts were enumerated microscopically at $\times 100$ magnification. As shown in Fig. 4, both KO and Trunc parasites exhibited significantly reduced levels of transmission competence compared to WT parasites. Oocyst numbers in mosquitoes infected with KO and Trunc parasites were 98% to 99% lower and 75 to 80% lower, respectively, than those seen with mosquitoes infected with WT parasites. Panels A and B of Fig. 4 show transmission results with two independent clones of KO and Trunc parasites. The differences in the oocyst burdens and in the percentages of infected mosquitoes between the WT and KO groups and the WT and Trunc groups were statistically significant ($P < 0.05$).

To ensure that the differences seen in the oocyst numbers were indeed due to gene disruption (KO or truncation) and not due to loss of infectiousness of parasites due to experimental manipulations performed during the transfection and cloning steps, we tested the transmission competence of parasite clones that went through the entire transfection process but that had a wild-type *PbZfp* genotype. As shown in Fig. 4C, these transfection control (Tc) parasites had numbers of oocysts comparable to those seen with the WT, indicating that the differences in the numbers of oocysts indicated in Fig. 4A and B were indeed due to disruption of *PbZfp* gene.

Additionally, we also compared gametocyte sex ratios in the blood of mice infected with WT, KO, and Trunc parasites on the day of mosquito infection (day 4). As shown in Fig. 4D, there was no significant association between the sex ratios and subsequent

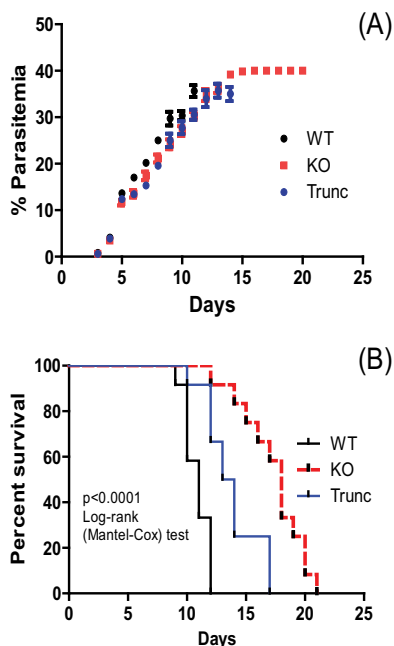


FIG 3 Comparison of *in vivo* asexual growth kinetics (A) and survival (B) of mice infected with WT, KO, and truncated *P. berghei*. Data shown are pooled from 12 mice per infection group (4 independent experiments, 3 mice per group for each parasite type). Blood smears prepared daily, beginning day 3 postinfection (10^5 infected red blood cells injected i.v.), were subjected to Giemsa staining for microscopy. The mice started to die beginning day 8 or 9, and the cages were observed twice daily to record death. A minimum of 500 to 1,000 red blood cells were counted to determine percent parasitemia [(infected RBC/total RBC) \times 100]. (A) Mean percentages of parasitemia \pm standard errors of the means (SEM) for all surviving mice on any given day. (B) Kaplan-Meier survival plots generated using GraphPad Prism software.

mosquito midgut stage development. Finally, we also compared ookinete formation differences between the WT, KO, and Trunc parasites using an *in vitro* ookinete development assay. On the day of mosquito feed, blood from infected mice was cultured for 24 to 30 h at 19°C and then examined microscopically. Figure 4D shows average ookinete counts for the three parasites and comparable morphologies of Giemsa-stained representative ookinetes (Fig. 4E).

Histone lysine methylation differences in WT, KO, and Trunc parasites. We next considered the possibility that PbZfp with 11 C₂H₂ ZnFs might affect histone methylation in the parasites. Purified parasites from mice infected with WT, KO, or Trunc parasites were analyzed by Western blotting. Lysates of parasites (10^6 per lane) were fractionated by 15% SDS-polyacrylamide gel electrophoresis (SDS-PAGE) and probed with a panel of histone lysine methylation- and histone lysine acetylation-specific antibodies. Anti-H3K4me₃, anti-H3K36me₃, and anti-H3K27me₃ antibodies showed strong reactivity with WT parasites (band just below the 17-kDa standard). However, all three antibodies failed to react with KO parasites (Fig. 5A). In sharp contrast to the histone methylation results, the WT and KO parasites showed comparable levels of reactivity, with antibodies recognizing H3K9ac, H3K14ac, and H4K16ac (Fig. 5B). Surprisingly, the levels of antibody reactivity with Trunc parasites lacking C₂H₂ ZnFs were comparable to those seen with WT parasites (Fig. 5A), suggesting that there is no apparent functional role of Zfd in histone modification.

To test the specificity of these antibodies and to revalidate these findings, we tested purified histones from WT, KO, and Trunc parasites. Figure 5C shows the purity of various histones (H2A, 18 kDa; H2B, 14 kDa; H3, 16 kDa; H4, 14 kDa) from WT, KO, and Trunc parasites. We then probed purified histones with various antibodies recognizing histone trimethylation and acetylation at specific lysine residues. Similarly to the results obtained with crude parasite lysates, all three methylation-specific antibodies recog-

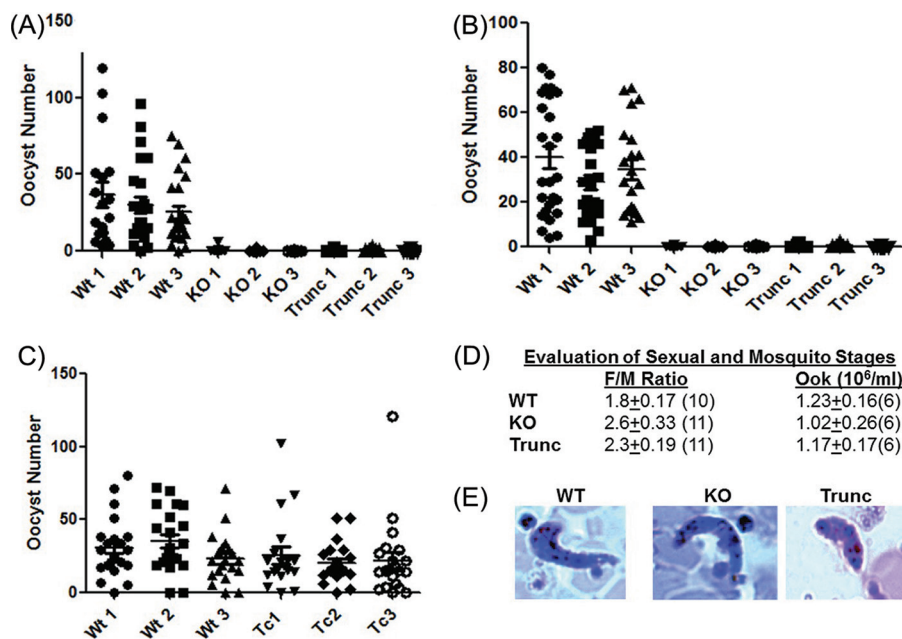


FIG 4 Comparison of transmission competence of WT, KO, and truncated parasites. Mice ($n = 3$ per group) were infected with WT, KO, and Trunc parasites and on day 4 postinfection were used to feed *A. stephensi* mosquitoes as described in Materials and Methods. Blood-fed mosquitoes were dissected (day 9 to day 11 post-blood feed), and midguts were examined microscopically (total magnification, $\times 100$) to determine the oocyst number in each midgut. Each column shows the oocyst distribution in the mosquitoes fed on an individual mouse. (A) Results from 3 mice per group infected with WT and one of the two clones of KO and Trunc parasites. (B) Repeat of analysis of transmission data using mice infected with WT and a second independent clonal line of KO and Trunc parasites. (C) Results obtained with WT and transfection control (Tc) parasites (parasites that possessed the WT locus but went through all the experimental manipulations used to obtain two different clonal KO and Trunc parasites). Blood smears on the day of mosquito infection were examined to determine gametocyte sex (female/male) ratios. Immediately after a mosquito feed, mice were bled to compare the characteristics of morphological development of ookinetes *in vitro*. (D) Results of analyses of female/male (F/M) gametocyte ratios and ookinete development (Ook), each averaged for observations pooled for 6 mice \pm SEM. (E) Representative Giemsa-stained ookinetes of WT, KO, and Trunc parasites.

nized histones from WT and Trunc parasites and, once again, no reactivity was seen with purified histones from KO parasites, demonstrating the inability of KO parasites to trimethylate H3K4, H3K36, or H3K27 (Fig. 5D). Purified histones from all three parasite lines (WT, KO, and Trunc) were strongly recognized by antibodies recognizing H3K14ac and H4K16ac (Fig. 5E).

Methyl methanesulfonate (MMS)-induced DNA damage response in WT, KO, and Trunc parasites. Previous studies have shown that chromatin modifier proteins such as PRDM9 (14, 15) target sites in the genome where DSB in DNA occur. Our observations confirming that PbZfp KO parasites completely lacked H3K4, H3K27, and H3K36 trimethylation led us to hypothesize that the KO parasites would exhibit reduced susceptibility to DNA-damaging agents. To test our hypothesis, we exposed WT, KO, and Trunc parasites for 6 h to various concentrations (0.05%, 0.005%, and 0.0005%) of the DNA-damaging agent MMS using conditions similar to those used in our previous studies with *P. falciparum* (35) followed by Comet assay analysis (18). There was an MMS dose-dependent increase in Olive tail moment (OTM) values for WT, KO, and Trunc parasites (Fig. 6, top). However, the OTM values in KO parasites exposed to 0.005% and 0.0005% concentrations of MMS were significantly lower than those seen with the WT and Trunc parasites, supporting our hypothesis that PbZfp disruption leads to reduced susceptibility to DNA damage responses. Even at the highest concentration (0.05%) of MMS, KO parasites still showed reduced DNA damage (P value = 0.054, approaching significance).

To quantify the percentage of damage in the parasites exposed to MMS, we counted the total number of cells, the total number of intact nuclei, and the total number of

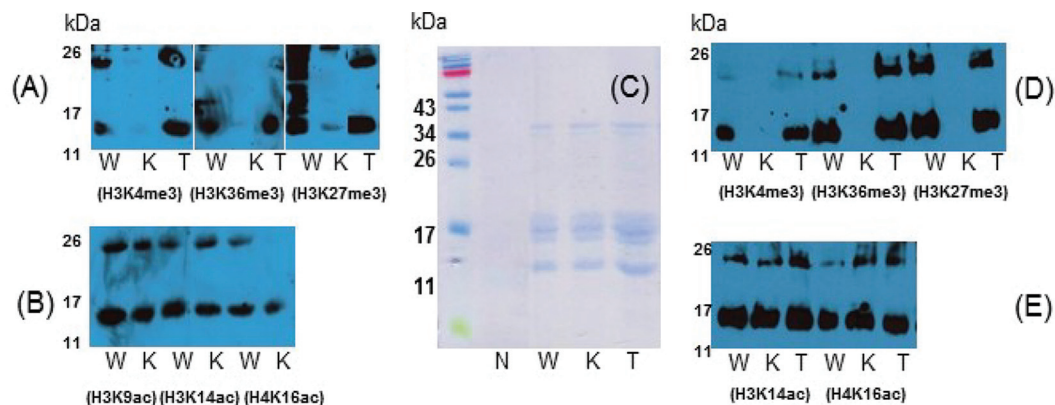


FIG 5 Histone methylation and acetylation patterns in WT, KO, and Trunc parasites. Blood from mice infected with WT (lanes W), KO (lanes K), and truncated (lanes T) parasites was passed through a cellulose column to remove leucocytes prior to saponin lysis and Western blot analysis. Samples (10^6 parasite equivalents per lane) were fractionated by 15% SDS-PAGE followed by transfer to a nitrocellulose membrane and probing with specific antibodies. (A and B) Reactivity patterns were determined using lysates of infected red blood cells with the indicated histone trimethylation (A)- and acetylation (B)-specific antibodies. We further purified histones from leucocyte depleted normal mouse red blood cells (N), WT (W), KO (K), and Trunc (T) parasites using an acid extraction procedure. (C) SDS-PAGE results obtained using a Coomassie blue-stained gel of each purified preparation. (D and E) Reactivity patterns determined using purified histones with the indicated histone trimethylation (D)- and acetylation (E)-specific antibodies.

Comets for each sample and then calculated the percentage of damaged cells (18). As seen in the bottom panel in Fig. 6, there was a dose-dependent increase in the percentage of damaged cells, with >95% damage at an MMS concentration of 0.05% in the WT and Trunc parasites. In contrast, KO parasites had only about 61% damage, once again demonstrating reduced susceptibility of KO parasites to the DNA-damaging

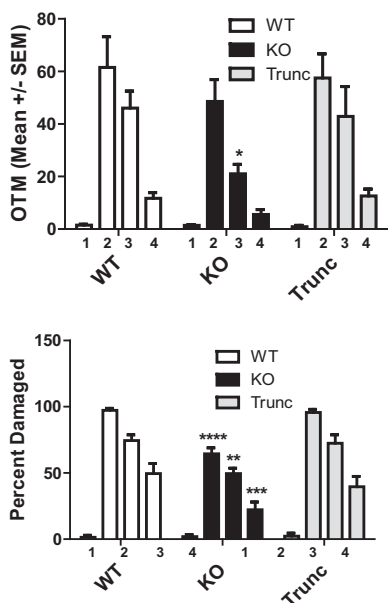


FIG 6 Susceptibility of WT, KO, and truncated *P. berghei* parasites in MMS-induced DNA damage response assay. Blood from infected mice was processed as described in Materials and Methods and tested in a MMS-induced DNA damage response assay previously optimized for similar studies in *P. falciparum* (36). Parasites in duplicate wells were treated with the indicated concentrations of MMS for 6 h followed by Comet assay analysis. The concentrations of MMS used were 0 (bars 1), 0.05% (bars 2), 0.005% (bars 3), and 0.0005% (bars 4). (Top panel) Olive tail moment (OTM) values were calculated as previously described (35) and averaged for each sample. (Bottom panel) Comets from each sample were further analyzed visually to estimate the proportion of damaged nuclei compared to the total number. Data were analyzed using GraphPad Prism software. Statistically significant differences ($P < 0.05$) between WT and KO parasites are indicated by an asterisk.

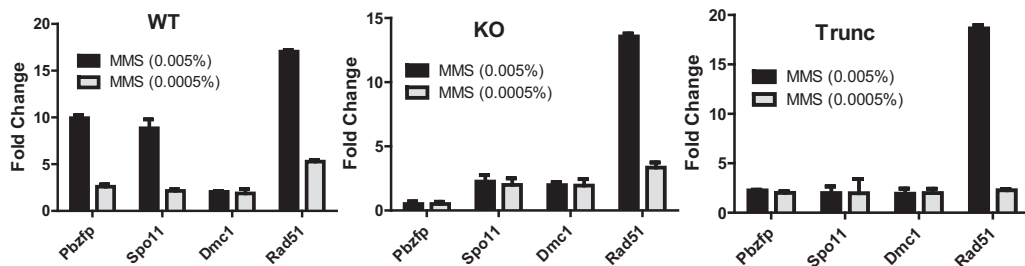


FIG 7 Transcriptional differences in WT parasites (left panel), KO parasites (middle panel), and truncated parasites (right panel) after exposure to MMS. An aliquot of parasite samples analyzed in Comet assays (Fig. 6) was used for transcriptional analysis by real-time RT-PCR. RNA was purified from parasites that were left untreated or were exposed to the indicated concentrations of MMS in duplicate wells, and purified RNA (1.0 μ g) was reverse transcribed as described in Materials and Methods. Three different amounts of cDNA (undiluted, diluted 1:10, and diluted 1:100) from each were analyzed by PCR using specific primers for *Pbzfp*, *PbSpo11*, *PbRad51*, and *PbDmc1* (Table S1) and a BioRad IQ5 real-time PCR detection system. *Pb18rRNA* gene served as an internal control. Relative C_T values from real-time PCR in the control and treated parasites were calculated by the Pfaff method, and fold change between untreated and treated samples was determined as previously described (35).

agent. These results also suggest a direct role for the region upstream of the C₂H₂ ZnFs in mediating susceptibility to DNA-damaging stimuli.

Induction of representative genes in the presence of DNA-damaging agent.

Previously, we showed that exposure to MMS induces expression of Rad51, Rad54, RPA1L, and RPA1S in *P. falciparum* (35, 36), indicating their role in DNA damage repair. In view of the fact that we observed reduced susceptibility of KO parasites to MMS, we studied the MMS-induced changes in the expression of select genes likely to be involved in DNA damage and repair mechanisms. We used quantitative real-time PCR to compare the relative amounts of and average threshold cycle ($\Delta\Delta C_T$) values for select genes in WT, KO, and Trunc parasites by the Pfaffl method (40). As shown in the left panel in Fig. 7, there were significant increases in the levels of expression of *Pbzfp*, *Spo11*, and *Rad51* (a mitotic recombinase gene) in WT parasites exposed to MMS. As expected, *Dmc1* (a meiotic recombinase gene and homolog of *Rad51*) was not induced by MMS in mitotically active blood stages. In KO and Trunc parasites, *Pbzfp* and *Spo11* were not induced, while they maintained normal inducibility of *Rad51* (Fig. 7, middle and right panels). This finding also suggests that *Spo11* probably acts in concert with *Pbzfp* in the parasites.

DISCUSSION

In organisms reproducing sexually, meiosis is an essential step responsible for generation of haploid gametes from diploid somatic cells. The combination of alignment of homologous chromosomes and the reciprocal exchange between two homologs creates new allelic combinations via HR. *Plasmodium* organisms in the vertebrate host and invertebrate mosquito vector are haploid throughout their life cycle except for a brief diploid zygote stage occurring in the mosquito midgut. Haploid male and female gametes fertilize in the mosquito midgut, and within a few hours the resulting zygote undergoes meiotic nuclear division, resulting in the development of haploid stages within developing oocysts. In mammals, DNA-binding C₂H₂ ZnFs and the H3K4 methyltransferase activity of the SET domain of PRDM9 play a major role in the identification of recombination hotspots in the genome during meiosis. H3K4 trimethylation leads to the recruitment of the evolutionarily conserved Spo11 (a topoisomerase-like enzyme) (41) to chromatin, which initiates DNA DSBs. Single-strand DNA tails created by DSBs allow further recruitment of Dmc1 and Rad51 proteins to facilitate genetic exchange via HR mechanisms. The processes of proper segregation of chromosomes during meiosis and formation of novel allelic genotypes depend upon genetic recombination occurring at unique sites termed “hotspots.”

We have previously described several molecular components involved in HR in *Plasmodium*, thus unequivocally demonstrating the presence of active functional HR

machinery in the parasite. These included homologs of Rad51, Rad54, RPA1 (in two forms, L and S), and meiotic recombinase Dmc1 in human and murine malaria parasites (35–37). However, the markers for chromosomal sites undergoing DNA DSBs during meiosis in *Plasmodium* are not well characterized. We investigated if PbZfp containing 11C₂H₂ ZnFs might mediate functions analogous to PRDM9 in mammals and might be important during meiosis and also an important determinant for transmission through the mosquitoes. We employed a reverse genetics approach to understand the functions of various protein domains in PbZfp. We developed *P. berghei* lacking full-length PbZfp (KO) and parasites expressing PbZfp lacking C-terminal Zfd (Trunc). We were able to successfully knock out the gene for PbZfp in the parasites, showing that it is not required for maintenance of erythrocytic asexual growth of parasites. While our studies did not find significant differences in proliferation rates among WT, KO, and Trunc parasites, a *P. falciparum* homolog of PbZfp was previously revealed by quantitative trait locus mapping analysis to be one of the several putative genes involved in regulating the duration of the cell cycle (42). It is noteworthy that the KO parasites seemed to be less virulent in mice despite showing peak parasitemia levels comparable to those seen with the mice infected with WT and Trunc parasites. The most striking phenotypic difference revealed was the loss of transmission competence of KO and Trunc parasites, thus pointing to a functional role of PbZfp during mosquito stage development.

Epigenetic mechanisms have been shown to play important roles in malaria parasite development, antigenic variation, *Var* gene silencing, and pathogenesis (43–52). We found that trimethylation of H3K4, H3K27, and H3K36 was completely blocked in PbZfp KO parasites. On the other hand, parasites expressing PbZfp lacking the C-terminal Zfd behaved like WT parasites, thus implicating the functionality of the N-terminal region of PbZfp, upstream of the Zfd, in mediating H3 lysine trimethylation. Interestingly, this was unique to histone 3 lysine methyl transferase activity since acetylation of histones (H3K9ac, H3K14ac, and H4K16ac) was not affected in either the KO parasites (Fig. 4B and E) or the truncated parasites. The simplest interpretation of the results would be that the N-terminal region of PbZfp recruits multiple histone methylases to chromatin. Paradoxically, genomic analysis has failed to identify any E(z) family H3K27 methylase in *P. falciparum*, and if the same holds true for *P. berghei*, it is puzzling that we detected H3K27 trimethylation in *P. berghei*. This observation suggests a possibility that 1 of the other SET domain proteins among the 9 to 10 found in *Plasmodium* species might play a role in mediating H3K27 trimethylation.

The KO parasites also exhibited trimethylation of H3K36. Not much is known about the functional role of H3K36me₃ in *Plasmodium*. In humans, H3K36me₃ has been shown to regulate DNA mismatch repair (53). Other recent studies have provided evidence of important mechanistic involvement of H3K36me₃ in the control of DNA damage signaling and DSB (54, 55). Because of the possible involvement of PbZfp in mosquito stage development, including meiosis, we compared the levels of susceptibility of DNA DSB formation in WT, KO, and Trunc parasites using MMS-induced DNA damage analysis and the Comet assay technique. PbZfp KO parasites were significantly less sensitive to MMS-induced DNA damage than WT and truncated parasites as revealed by lower OTM values and percentages of accumulation of damaged nuclei upon exposure to MMS. Reduced susceptibility to MMS-induced DNA damage was further substantiated by quantitative RT-PCR (qRT-PCR) analysis. MMS caused induction of *PbZfp*, *Spo11*, and *PbRad51* in WT parasites. Not too surprising, *PbDmc1* encoding a meiotic recombinase was not induced by MMS in mitotically active blood-stage parasites. In contrast, *Spo11* was not induced in the KO and Trunc parasites, providing additional support for findings of reduced susceptibility to MMS-induced DNA damage in Comet assays. The fact that the induction of *PbRad51*, a key HR repair component, was not affected in the KO and Trunc parasites suggests that these parasites maintain efficient HR repair machinery independently of PbZfp, resulting in efficient repair of damaged DNA. The results presented here indicate a key biological role for a ZnF protein during *Plasmodium* transmission via mosquitoes on one hand and regulation of

epigenetic modifications and susceptibility of the parasite to DNA-damaging conditions on the other.

MATERIALS AND METHODS

Identification of PbZfp gene in *P. berghei*. *Plasmodium* parasites, like other apicomplexans, have relatively few transcription factors and, in contrast to animals, almost none with C₂H₂ ZnFs (56). Nevertheless, they contain a well-conserved C₂H₂ ZnF protein present across *Plasmodium* species, including *P. falciparum*, identified using a PSI-BLAST sequence profile for C₂H₂ ZnFs (39). In *P. berghei*, this protein is encoded by a 3,747-bp open reading frame on chromosome 6 (PBANKA_060770). The product of this gene (termed PbZfp here) has been annotated "putative Krox1-like transcription factor" in the PlasmoDB although it has no specific relationship to the mammalian Krox1 protein beyond the presence of multiple C₂H₂ ZnFs (Fig. 1A). PbZfp contains 11 C₂H₂ ZnFs in the C-terminal region extending from approximately amino acid 800 to amino acid 1248.

Plasmids for gene targeting in *P. berghei*. A gene knockout plasmid (pB3D backbone) was constructed by sequential insertion of following sequences: (i) PCR-amplified (574 bp; primers 778/779; pDEF plasmid template) *P. berghei* EF1 α promoter (*PbEF1 α*) between BamHI and EcoRI sites; (ii) PCR-amplified (711 bp; primers 776/777; pB3D-mCherry template) *mCherry* between EcoRI and EcoRV sites; (iii) PCR-amplified (450 bp; primers 780/781; pDEF plasmid) *PbDHFR 3'utr* in the EcoRV site; (iv) PCR-amplified (755 bp; primers 809/810; *P. berghei* genomic DNA template) *PbZfp 3'utr* between HindIII and KpnI sites; and (v) PCR-amplified (773 bp; primers 803/804; *P. berghei* genomic DNA template) *PbZfp 5'utr* in the SacII and SpeI sites. The *PbZfp* gene encodes a protein containing a Zfd consisting of 11 C₂H₂ zinc fingers toward the C terminus (Fig. 1A). To analyze the functional role of this region, we also developed a second gene-targeting plasmid to generate parasites expressing truncated PbZfp lacking Zfd. First, a PbZfp coding sequence corresponding to amino acids 568 to 862 was obtained by PCR amplification (882 bp; primers 805/806; *P. berghei* genomic DNA template) and cloned between SacII and SpeI sites of the plasmid obtained after step iv (see above). Next, we amplified a PfZfp sequence (610 bp in length; primers 823/824, *P. berghei* genomic DNA template) comprised of the last two codons (including the stop codon) and the 3' *utr* of *PbZfp* immediately downstream for insertion in the SpeI and BamHI sites. The plasmid pB3D encodes *Toxoplasma gondii* DHFR-TS, which confers resistance to pyrimethamine and allows selection of transfected parasites. Primer details are given in Table S1 in the supplemental material. At each cloning step, plasmids were verified by restriction digestion and sequence analysis.

Transfection and diagnostic PCR analysis of PbZfp knockout parasites and truncated parasites. For transfection, plasmid DNA was purified using a plasmid Maxi kit (Qiagen) and linearized by digestion with SacII and KpnI. Linearized DNA (10 micrograms) and an Amaxa human T cell nucleofector kit (U033 settings) were used for each transfection. Transfected parasites were injected i.v. into naive Swiss-Webster mice, and mice were put on drinking water containing pyrimethamine (70 μ g/ml) 24 h posttransfection to select for drug-resistant transformants. Genotypes and various recombination events in the drug-resistant parasites were characterized by PCR analysis prior to and after cloning by limiting dilution. Two clones of parasites with PfZfp knockout (KO) and PfZfp truncation (Trunc) were selected from two independent transfections for these studies.

Reverse transcriptase PCR to examine expression of PbZfp. Total RNA was extracted from WT, KO, and Trunc parasites obtained from infected Swiss-Webster mice using Trizol reagent (Invitrogen), and concentrations were determined using a NanoDrop instrument (model 2000/2000c). RNA (1 microgram) was reverse transcribed using a Qiagen One-Step RT-PCR kit, and the resulting cDNAs were subjected to PCR amplification for 35 cycles using gene-specific primers (Table S1). Control reactions were carried out without a reverse transcriptase step to confirm that no genomic DNA contamination was present in the RNA samples. The products were run on a 1% agarose gel and stained with ethidium bromide.

Characterization of asexual growth kinetics, ookinete formation, and transmission to mosquitoes. Swiss-Webster mice (female, 6 to 8 weeks old) were infected i.v. with 10⁵ infected red blood cells (RBCs) of WT, KO, and Trunc parasites (3 mice per group). Beginning on day 3, parasitemia was monitored daily by examining Giemsa-stained thin blood smears. Mice were monitored twice daily to record any mortality. Blood smears were also examined on day 4 or day 5 postinfection for determination of the relative abundances of male and female gametocytes. To compare ookinete stage development, blood was drawn from mice infected with WT, KO, or Trunc parasites with approximately equivalent levels of gametocytemia on day 4 postinfection. The blood was then diluted 1:5 in RPMI 1640 medium supplemented with 10% fetal bovine serum and incubated at 19°C for 24 to 30 h. Thin smears were prepared and subjected to Giemsa staining to examine the morphology of ookinetes. Multiple replicates of cultured diluted blood were used to enumerate ookinetes by the use of a hemocytometer at \times 400 magnification, and counts were expressed as numbers of ookinetes per milliliter. Female *A. stephensi* mosquitoes (4-to-5-day-old adults; $n = 25$ to 30 per mouse) starved for 4 to 5 h were allowed to engorge on infected mice (typically on day 4 postinfection) for 30 min. Blood-fed mosquitoes were maintained on 10% dextrose in an incubator at 70% to 80% relative humidity and 19°C (optimal for *P. berghei* development in the mosquitoes). Mosquitoes were dissected on days 9 to 11 to determine the oocyst load in the midgut.

Purification of histones. Histones were purified from parasites using an acid extraction method (57, 58) with minor modifications. Briefly, 1 to 3 \times 10⁹ parasites were harvested from mice infected with *P. berghei* (WT, KO, or Trunc). The parasite pellets were washed two times with cold phosphate-buffered saline (PBS) and two times with a buffer (25 mM Tris-HCl [pH 7.8], 1 mM EDTA, 0.2% Nonidet P-40) to remove hemoglobin. After washing three times with 0.8 M NaCl, the pellets were treated two times with

0.25 M HCl to extract histones. Acid-soluble fractions were pooled and precipitated with equal volumes of 25% trichloroacetic acid on ice for 1 h. Precipitated histones were collected by centrifugation at $12,000 \times g$ for 15 min at 4°C, washed with 500 μ l of acetone, and air dried. Samples were resuspended in 100 μ l of PBS (pH 7.0) and analyzed by 17.5% SDS-polyacrylamide gel electrophoresis (SDS-PAGE) and Western blotting using antibodies against histone 3 and histone 4.

Analysis of histone methylation and acetylation. Swiss-Webster mice were infected (i.v.) with 10^6 parasites (WT, KO, or Trunc) (5 mice/group) and bled when the parasitemia reached $>10\%$. Parasites were freed from infected red cells by 0.01% saponin treatment (5 min on ice), washed two times in ice-cold PBS, and lysed using SDS-PAGE sample buffer (15 min at room temperature). The lysates were centrifuged (10,000 rpm, 10 min), and the supernatants were heated (95°C, 5 min) prior to SDS-PAGE. Samples were probed using Western blotting and a 1:10,000 dilution of mouse anti-H3K4me3 (histone H3 trimethyl K4; clone mAbcam 1012), mouse anti-H3K27me3 (histone H3 trimethyl K27; clone mAbcam 6002), rabbit anti-H3K36me3 (histone H3 trimethyl K36; ab9050), rabbit anti-H3K9ac (histone H3 acetyl K9; ab10812), rabbit anti-H3K14ac (histone H3 acetyl K14; ab52946), and mouse anti-H4K16 acetyl (histone H4 acetyl Lys16; Millipore catalog no. 05-1232) antibodies and ECL-based detection methods (Amersham Pharmacia Biotech). In addition to parasite lysates, purified histones were also tested for validation of specific modifications revealed by Western blotting.

Evaluation of DNA damage by Comet assay. Swiss-Webster mice were infected (i.v.) with 10^5 WT, KO, or Trunc parasites (5 mice/group). Mice were bled by cardiac puncture, and the blood was passed through cellulose columns to remove white blood cells (WBCs) and resuspended at a hematocrit level of 5% in RPMI 1640 medium containing 20% fetal bovine serum and gentamicin. Infected mouse blood was plated in duplicate wells in 6-well tissue culture plates with various concentrations of methyl methane-sulfonate (MMS) (0%, 0.05%, 0.005%, and 0.0005%). Parasites were incubated for 6 h (36), lysed with 0.05% saponin, washed with PBS (pH 7.4), and finally resuspended in 1.0 ml PBS for Comet assay analysis (35). Diluted cells (30 μ l) were mixed with 300 μ l Comet LMAgarose (Trevigen, Gaithersburg, MD) (1% low-melting-temperature agarose), and the mixture was added to wells of Trevigen slides, incubated at 4°C for 30 min, and immersed in chilled lysis solution (Trevigen) at 4°C for 60 min. Slides were then transferred to a clean tray and immersed in alkaline lysis solution (200 mM NaOH and 1 mM EDTA). Lysed cells were electrophoresed for 30 min at 1 V/cm in $1 \times$ Tris-borate-EDTA (TBE) buffer, followed by fixation in 70% ethanol and drying overnight. Wells were stained with 50 μ l freshly prepared SYBR green I and photographed at $\times 200$ magnification using a Nikon Eclipse 80i (Nikon) high-performance camera with Senciscam QE (Cooke Corporation). Results corresponding to Comet head and tail length, head and tail percent intensity, tail migration, and Olive tail moment (OTM) (the product of the tail length and the fraction of total DNA in the tail) were scored using Comet assay IV software. For each sample (control or MMS treatment), three replicates were performed and averages of their OTM values were used for data analysis. Comets were also analyzed visually to score round undamaged (intact) and Comet (damaged) cells to calculate percent damage.

Real-time qPCR analysis. RNA from infected red blood cells from mice infected with parasites (WT, KO, Trunc) was purified using Trizol reagent (Invitrogen) and used for cDNA synthesis as described above. Samples for quantitative PCR (qPCR) analysis were prepared in IQ SYBR green Supermix, containing SYBR green dye, iTaq DNA polymerase, deoxynucleoside triphosphates (dNTPs) and buffers (Bio-Rad), 0.4 μ M gene-specific oligonucleotide primers (Table S1), and a 1:100 dilution of the cDNA reaction products. Amplification was performed on a Bio-Rad IQ5 real-time PCR detection system using 95°C for 2 min for the initial denaturation and enzyme activation followed by further incubation at 95°C for 3 min and 45 cycles of 95°C for 30 s, 50°C for 30 s, and 72°C for 30 s. Primers for the *P. berghei* 18S rRNA gene (PlasmoDB.org gene identifier [ID]: PBANKA_0521221) were used as an internal control. Each sample was analyzed as three independent replicates, and the average values were used for data analysis.

Data analysis and statistical evaluation. GraphPad Prism Software (GraphPad Software, Inc., CA) was used for statistical analyses of the data. Regression analysis was used to determine the differences in asexual growth kinetics of WT, KO, and Trunc parasites. The Mann-Whitney *U* test was used to compare the oocyst counts from the WT, KO, and Trunc parasites.

For analysis of the OTM values from the WT, KO, and Trunc parasites, a Shapiro-Wilk test was performed first to establish the normalcy of the data. Further, a Mann-Whitney *U* test was performed to determine two-tailed *P* values. Relative threshold cycle (C_T) values from RT-PCR analysis of the induced and uninduced samples were calculated by using the Pfaffl method (40), and $\Delta\Delta C_T$ values were used to estimate fold change as previously described (35). *P* values of less than 0.05 were considered statistically significant.

SUPPLEMENTAL MATERIAL

Supplemental material for this article may be found at <https://doi.org/10.1128/mBio.01298-17>.

FIG S1, TIF file, 0.2 MB.

TABLE S1, DOCX file, 0.02 MB.

ACKNOWLEDGMENTS

We thank members of the Kumar laboratory for critical discussions during various phases of the work and Melody C. Baddoo for the Comet assays performed in the core

laboratory. We also thank C. Qiu and L. Schrader for the kind gift of various antibodies used in epigenetic modification analysis.

Initial financial support for these studies was from NIH grant R56 AI68052. The Comet assay core laboratory is supported by NIH grants from the National Center for Research Resources (5P20RR020152) and the NIGMS (8P20GM103518).

REFERENCES

1. WHO. 2015. World Malaria Report 2015. World Health Organization, Geneva, Switzerland. <http://www.who.int/malaria/publications/world-malaria-report-2015/report/en>.
2. Sinden RE, Hartley RH. 1985. Identification of the meiotic division of malarial parasites. *J Protozool* 32:742–744. <https://doi.org/10.1111/j.1550-7408.1985.tb03113.x>.
3. Babiker HA, Ranford-Cartwright LC, Currie D, Charlwood JD, Billingsley P, Teuscher T, Walliker D. 1994. Random mating in a natural population of the malaria parasite *Plasmodium falciparum*. *Parasitology* 109:413–421. <https://doi.org/10.1017/S0031182000080665>.
4. Day KP, Koella JC, Nee S, Gupta S, Read AF. 1992. Population genetics and dynamics of *Plasmodium falciparum*: an ecological view. *Parasitology* 104:S35–S52. <https://doi.org/10.1017/S0031182000075235>.
5. Paul REL, Day KP. 1998. Mating patterns of *Plasmodium falciparum*. *Parasitology Today* 14:197–202. [https://doi.org/10.1016/S0169-4758\(98\)01226-5](https://doi.org/10.1016/S0169-4758(98)01226-5).
6. Walliker D, Quakyi IA, Wellems TE, McCutchan TF, Szarfman A, London WT, Corcoran LM, Burkot TR, Carter R. 1987. Genetic analysis of the human malaria parasite *Plasmodium falciparum*. *Science* 236:1661–1666. <https://doi.org/10.1126/science.3299700>.
7. Petronczki M, Siomos MF, Nasmyth K. 2003. Un ménage à quatre: the molecular biology of chromosome segregation in meiosis. *Cell* 112:423–440. [https://doi.org/10.1016/S0092-8674\(03\)00083-7](https://doi.org/10.1016/S0092-8674(03)00083-7).
8. Lichten M, Goldman AS. 1995. Meiotic recombination hotspots. *Annu Rev Genet* 29:423–444. <https://doi.org/10.1146/annurev.ge.29.120195.002231>.
9. Myers S, Bottolo L, Freeman C, McVean G, Donnelly P. 2005. A fine-scale map of recombination rates and hotspots across the human genome. *Science* 310:321–324. <https://doi.org/10.1126/science.1117196>.
10. Winckler W, Myers SR, Richter DJ, Onofrio RC, McDonald GJ, Bontrop RE, McVean GA, Gabriel SB, Reich D, Donnelly P, Altshuler D. 2005. Comparison of fine-scale recombination rates in humans and chimpanzees. *Science* 308:107–111. <https://doi.org/10.1126/science.1105322>.
11. Shiroishi T, Koide T, Yoshino M, Sagai T, Moriwaki K. 1995. Hotspots of homologous recombination in mouse meiosis. *Adv Biophys* 31:119–132. [https://doi.org/10.1016/0065-227X\(95\)99387-5](https://doi.org/10.1016/0065-227X(95)99387-5).
12. Buard J, Barthès P, Grey C, de Massy B. 2009. Distinct histone modifications define initiation and repair of meiotic recombination in the mouse. *EMBO J* 28:2616–2624. <https://doi.org/10.1038/emboj.2009.207>.
13. Borde V, Robine N, Lin W, Bonfils S, Géli V, Nicolas A. 2009. Histone H3 lysine 4 trimethylation marks meiotic recombination initiation sites. *EMBO J* 28:99–111. <https://doi.org/10.1038/emboj.2008.257>.
14. Baudat F, Buard J, Grey C, Fedel-Alon A, Ober C, Przeworski M, Coop G, de Massy B. 2010. PRDM9 is a major determinant of meiotic recombination hotspots in humans and mice. *Science* 327:836–840. <https://doi.org/10.1126/science.1183439>.
15. Myers S, Bowden R, Tumian A, Bontrop RE, Freeman C, MacFie TS, McVean G, Donnelly P. 2010. Drive against hotspot motifs in primates implicates the PRDM9 gene in meiotic recombination. *Science* 327:876–879. <https://doi.org/10.1126/science.1182363>.
16. Parvanov ED, Petkov PM, Paigen K. 2010. Prdm9 controls activation of mammalian recombination hotspots. *Science* 327:835. <https://doi.org/10.1126/science.1181495>.
17. Barthès P, Buard J, De Massy B. 2011. Epigenetic factors and regulation of meiotic recombination in mammals, p 119–156. *In* Epigenetics and human health. Springer, New York, NY. https://doi.org/10.1007/978-3-642-14773-9_6.
18. Aravind L, Abhiman S, Iyer LM. 2011. Natural history of the eukaryotic chromatin protein methylation system. *Prog Mol Biol Transl Sci* 101:105–176. <https://doi.org/10.1016/B978-0-12-387685-0.00004-4>.
19. Powers NR, Parvanov ED, Baker CL, Walker M, Petkov PM, Paigen K. 2016. The meiotic recombination activator PRDM9 trimethylates both H3K36 and H3K4 at recombination hotspots in vivo. *PLoS Genet* 12:e1006146. <https://doi.org/10.1371/journal.pgen.1006146>.
20. Jenuwein T. 2001. Re-SET-ting heterochromatin by histone methyltransferases. *Trends Cell Biol* 11:266–273. [https://doi.org/10.1016/S0962-8924\(01\)02001-3](https://doi.org/10.1016/S0962-8924(01)02001-3).
21. Branden C, Tooze J. 1991. Structural motifs of eukaryotic transcription factors, p 113–127. *In* Introduction to protein structure. Garland Publishing, New York, NY.
22. Razin SV, Borunova VV, Maksimenko OG, Kantidze OL. 2012. Cys2His2 zinc finger protein family: classification, functions, and major members. *Biochemistry* 77:217–226. <https://doi.org/10.1134/S0006297912030017>.
23. Berger SL. 2002. Histone modifications in transcriptional regulation. *Curr Opin Genet Dev* 12:142–148. [https://doi.org/10.1016/S0959-437X\(02\)00279-4](https://doi.org/10.1016/S0959-437X(02)00279-4).
24. Black JC, Van Rechem C, Whetstone JR. 2012. Histone lysine methylation dynamics: establishment, regulation, and biological impact. *Mol Cell* 48:491–507. <https://doi.org/10.1016/j.molcel.2012.11.006>.
25. Wang X, Zhu WG. 2008. Advances in histone methyltransferases and histone demethylases. *Ai Zheng* 27:1018–1025. (In Chinese.).
26. Jha DK, Pfister SX, Humphrey TC, Strahl BD. 2014. SET-ting the stage for DNA repair. *Nat Struct Mol Biol* 21:655–657. <https://doi.org/10.1038/nsmb.2866>.
27. Richardson C, Horikoshi N, Pandita TK. 2004. The role of the DNA double-strand break response network in meiosis. *DNA Repair* 3:1149–1164. <https://doi.org/10.1016/j.dnarep.2004.05.007>.
28. Baudat F, Imai Y, de Massy B. 2013. Meiotic recombination in mammals: localization and regulation. *Nat Rev Genet* 14:794–806. <https://doi.org/10.1038/nrg3573>.
29. Pan J, Keeney S. 2007. Molecular cartography: mapping the landscape of meiotic recombination. *PLoS Biol* 5:e333. <https://doi.org/10.1371/journal.pbio.0050333>.
30. Jiang H, Li N, Gopalan V, Zilversmit MM, Varma S, Nagarajan V, Li J, Mu J, Hayton K, Henschen B, Yi M, Stephens R, McVean G, Awadalla P, Wellems TE, Su XZ. 2011. High recombination rates and hotspots in a *Plasmodium falciparum* genetic cross. *Genome Biol* 12:R33. <https://doi.org/10.1186/gb-2011-12-4-r33>.
31. Mu J, Awadalla P, Duan J, McGee KM, Joy DA, McVean GA, Su XZ. 2005. Recombination hotspots and population structure in *Plasmodium falciparum*. *PLoS Biol* 3:e335. <https://doi.org/10.1371/journal.pbio.0030335>.
32. Li J, Pattaradilokrat S, Zhu F, Jiang H, Liu S, Hong L, Fu Y, Koo L, Xu W, Pan W, Carlton JM, Kaneko O, Carter R, Wootton JC, Su XZ. 2011. Linkage maps from multiple genetic crosses and loci linked to growth-related virulent phenotype in *Plasmodium yoelii*. *Proc Natl Acad Sci U S A* 108:E374–E382. <https://doi.org/10.1073/pnas.1102261108>.
33. Su XZ, Wootton JC. 2004. Genetic mapping in the human malaria parasite *Plasmodium falciparum*. *Mol Microbiol* 53:1573–1582. <https://doi.org/10.1111/j.1365-2958.2004.04270.x>.
34. Bhattacharyya MK, Bhattacharyya nee Deb S, Jayabalasingham B, Kumar N. 2005. Characterization of kinetics of DNA strand-exchange and ATP hydrolysis activities of recombinant PfRad51, a *Plasmodium falciparum* recombinase. *Mol Biochem Parasitol* 139:33–39.
35. Gopalakrishnan AM, Kumar N. 2013. Opposing roles for two molecular forms of replication protein A in Rad51-Rad54-mediated DNA recombination in *Plasmodium falciparum*. *mBio* 4:e00252-13. <https://doi.org/10.1128/mBio.00252-13>.
36. Bhattacharyya MK, Kumar N. 2003. Identification and molecular characterisation of DNA damaging agent induced expression of *Plasmodium falciparum* recombination protein PfRad51. *Int J Parasitol* 33:1385–1392. [https://doi.org/10.1016/S0020-7519\(03\)00212-1](https://doi.org/10.1016/S0020-7519(03)00212-1).
37. Mlambo G, Coppens I, Kumar N. 2012. Aberrant sporogonic development of Dmc1 (a meiotic recombinase) deficient *Plasmodium berghei* parasites. *PLoS One* 7:e52480. <https://doi.org/10.1371/journal.pone.0052480>.

38. Pease BN, Huttlin EL, Jedrychowski MP, Talevich E, Harmon J, Dillman T, Kannan N, Doerig C, Chakrabarti R, Gygi SP, Chakrabarti D. 2013. Global analysis of protein expression and phosphorylation of three stages of *Plasmodium falciparum* intraerythrocytic development. *J Proteome Res* 12:4028–4045. <https://doi.org/10.1021/pr400394g>.
39. Iyer LM, Anantharaman V, Wolf MY, Aravind L. 2008. Comparative genomics of transcription factors and chromatin proteins in parasitic protists and other eukaryotes. *Int J Parasitol* 38:1–31. <https://doi.org/10.1016/j.ijpara.2007.07.018>.
40. Pfaffl MW. 2001. A new mathematical model for relative quantification in real-time RT-PCR. *Nucleic Acids Res* 29:e45. <https://doi.org/10.1093/nar/29.9.e45>.
41. Keeney S. 2008. Spo11 and the formation of DNA double-strand breaks in meiosis. *Genome Dyn Stab* 2:81–123. https://doi.org/10.1007/7050_2007_026.
42. Reilly Ayala HBR, Wacker MA, Siwo G, Ferdig MT. 2010. Quantitative trait loci mapping reveals candidate pathways regulating cell cycle duration in *Plasmodium falciparum*. *BMC Genomics* 11:577. <https://doi.org/10.1186/1471-2164-11-577>.
43. Choekajorn T, Dzikowski R, Frank M, Li F, Jiwani AZ, Hartl DL, Deitsch KW. 2007. Epigenetic memory at malaria virulence genes. *Proc Natl Acad Sci U S A* 104:899–902. <https://doi.org/10.1073/pnas.0609084103>.
44. Cui L, Miao J, Furuya T, Li X, Su X-z, Cui L. 2007. PfGCN5-mediated histone H3 acetylation plays a key role in gene expression in *Plasmodium falciparum*. *Eukaryot Cell* 6:1219–1227. <https://doi.org/10.1128/EC.00062-07>.
45. Sautel CF, Cannella D, Bastien O, Kieffer S, Aldebert D, Garin J, Tardieux I, Belrhali H, Hakimi MA. 2007. SET8-mediated methylations of histone H4 lysine 20 mark silent heterochromatic domains in apicomplexan genomes. *Mol Cell Biol* 27:5711–5724. <https://doi.org/10.1128/MCB.00482-07>.
46. Duraisingh MT, Voss TS, Marty AJ, Duffy MF, Good RT, Thompson JK, Freitas-Junior LH, Scherf A, Crabb BS, Cowman AF. 2005. Heterochromatin silencing and locus repositioning linked to regulation of virulence genes in *Plasmodium falciparum*. *Cell* 121:13–24. <https://doi.org/10.1016/j.cell.2005.01.036>.
47. Freitas-Junior LH, Hernandez-Rivas R, Ralph SA, Montiel-Condado D, Ruvalcaba-Salazar OK, Rojas-Meza AP, Mancio-Silva L, Leal-Silvestre RJ, Gontijo AM, Shorte S, Scherf A. 2005. Telomeric heterochromatin propagation and histone acetylation control mutually exclusive expression of antigenic variation genes in malaria parasites. *Cell* 121:25–36. <https://doi.org/10.1016/j.cell.2005.01.037>.
48. Lopez-Rubio JJ, Gontijo AM, Nunes MC, Issar N, Hernandez Rivas R, Scherf A. 2007. 5' Flanking region of *var* genes nucleate histone modification patterns linked to phenotypic inheritance of virulence traits in malaria parasites. *Mol Microbiol* 66:1296–1305. <https://doi.org/10.1111/j.1365-2958.2007.06009.x>.
49. Jiang L, Mu J, Zhang Q, Ni T, Srinivasan P, Rayavara K, Yang W, Turner L, Lavstsen T, Theander TG, Peng W, Wei G, Jing Q, Wakabayashi Y, Bansal A, Luo Y, Ribeiro JM, Scherf A, Aravind L, Zhu J, Zhao K, Miller LH. 2013. PfSETvs methylation of histone H3K36 represses virulence genes in *Plasmodium falciparum*. *Nature* 499:223–227. <https://doi.org/10.1038/nature12361>.
50. Coleman BI, Skillman KM, Jiang RHY, Childs LM, Altenhofen LM, Ganter M, Leung Y, Goldowitz I, Kafsack BFC, Marti M, Llinás M, Buckee CO, Duraisingh MT. 2014. A *Plasmodium falciparum* histone deacetylase regulates antigenic variation and gametocyte conversion. *Cell Host Microbe* 16:177–186. <https://doi.org/10.1016/j.chom.2014.06.014>.
51. Chaal BK, Gupta AP, Wastuwidyaningtyas BD, Luah YH, Bozdech Z. 2010. Histone deacetylases play a major role in the transcriptional regulation of the *Plasmodium falciparum* life cycle. *PLoS Pathog* 6:e1000737. <https://doi.org/10.1371/journal.ppat.1000737>.
52. Ukaegbu UE, Kishore SP, Kwiatkowski DL, Pandarinath C, Dahan-Pasternak N, Dzikowski R, Deitsch KW. 2014. Recruitment of PfSET2 by RNA polymerase II to variant antigen encoding loci contributes to antigenic variation in *P. falciparum*. *PLoS Pathog* 10:e1003854. <https://doi.org/10.1371/journal.ppat.1003854>.
53. Li F, Mao G, Tong D, Huang J, Gu L, Yang W, Li GM. 2013. The histone mark H3K36me3 regulates human DNA mismatch repair through its interaction with MutS α . *Cell* 153:590–600. <https://doi.org/10.1016/j.cell.2013.03.025>.
54. Jha DK, Strahl BD. 2014. An RNA polymerase II-coupled function for histone H3K36 methylation in checkpoint activation and DSB repair. *Nat Commun* 5:3965. <https://doi.org/10.1038/ncomms4965>.
55. Carvalho S, Vitor AC, Sridhara SC, Martins FB, Raposo AC, Desterro JM, Ferreira J, de Almeida SF. 2014. SETD2 is required for DNA double-strand break repair and activation of the p53-mediated checkpoint. *Elife* 3:e02482. <https://doi.org/10.7554/eLife.02482>.
56. Aravind L, Anantharaman V, Venancio TM. 2009. Apprehending multicellularity: regulatory networks, genomics, and evolution. *Birth Defects Res C Embryo Today* 87:143–164. <https://doi.org/10.1002/bdrc.20153>.
57. Longhurst HJ, Holder AA. 1997. The histones of *Plasmodium falciparum*: identification, purification and a possible role in the pathology of malaria. *Parasitology* 114:413–419. <https://doi.org/10.1017/S0031182096008621>.
58. Miao J, Fan Q, Cui L, Li J, Li J, Cui L. 2006. The malaria parasite *Plasmodium falciparum* histones: organization, expression, and acetylation. *Gene* 369:53–65. <https://doi.org/10.1016/j.gene.2005.10.022>.